Biosensors and Bioelectronics 130 (2019) 293–298

Contents lists available at ScienceDirect

Biosensors and Bioelectronics

journal homepage: www.elsevier.com/locate/bios

Enhanced surface plasmon resonance (SPR) signals based on immobilization of core-shell nanoparticles incorporated boron nitride nanosheets: Development of molecularly imprinted SPR nanosensor for anticancer drug, etoposide

Abdullah Özkan[a], Necip Atar[b], Mehmet Lütfi Yola[c,*]

[a] Iskenderun Technical University, Faculty of Engineering and Natural Sciences, Department of Petroleum and Natural Gas, Hatay, Turkey
[b] Pamukkale University, Faculty of Engineering, Department of Chemical Engineering, Denizli, Turkey
[c] Iskenderun Technical University, Faculty of Engineering and Natural Sciences, Department of Biomedical Engineering, Hatay, Turkey

ARTICLE INFO

Keywords:
Molecular imprinted nanosensor
Etoposide
Core-shell nanoparticles
Hexagonal boron nitride
Urine sample

ABSTRACT

An effective SPR nanosensor based on core-shell nanoparticles (Ag@AuNPs) incorporated hexagonal boron nitride (HBN) nanosheets and molecularly imprinted polymer (MIP) was presented for etoposide (ETO) detection. Scanning electron microscope (SEM), transmission electron microscope (TEM), x-ray diffraction (XRD) method, cyclic voltammetry (CV), electrochemical impedance spectroscopy (EIS), fourier transform infrared (FTIR) spectroscopy and atomic force microscopy (AFM) methods were utilized for all characterizations of nanomaterials and polymer surfaces. ETO imprinted SPR nanosensor based on Ag@AuNPs-HBN nanocomposite was developed in the presence of poly(2-hydroxyethyl methacrylate-methacryloylamidoglutamic acid) [p(HEMA-MAGA)]. The results of the study have revealed that 0.001–1.00 ng mL^{-1} (1.70×10^{-12}–1.70×10^{-9} M) and 0.00025 ng mL^{-1} (4.25×10^{-13} M) were found as the linearity range and the detection limit (LOD). Furthermore, the prepared SPR nanosensor was examined in terms of stability, repeatability and selectivity. Finally, the imprinted SPR nanosensor was applied to the urine samples having high recovery.

1. Introduction

ETO is one of the most important anticancer drugs and utilized for treating various types of cancers. It is a derivative of podophyllotoxin which is able to treat lung cancer, neuroblastoma and ovarian cancer (Nguyen et al., 2016; Pang et al., 2001). However, the treatment mechanism is unclear on medical applications. Because of this situation, the clinical applications are limited owing to the side effects (Poole et al., 2006; Xu et al., 2012). Several analytical procedures like ultra performance liquid chromatography-tandem mass spectrometry (UPLC-MS/MS), high performance thin layer chromatographic (HPTLC) and reverse-phase high-performance liquid chromatography (RP-HPLC) are used to determine ETO (Gong et al., 2017; Kamal et al., 2017). Due to the high selectivity and mechanical properties, the molecularly imprinted polymers (MIP) are the most effective means for the preparation of synthetic recognition elements (Stobiecka et al., 2009; Yola et al., 2016). MIPs are widely used in pharmaceutical industry, agriculture, food and environmental science as a recognition element. The development of MIP-based sensors is one of the most challenging issues in recent years (Medetalibeyoğlu et al., 2018). Due to these reasons, more sensitive, simple and selective sensors based on nanomaterials are needed in terms of environmental safety (Hepel and Stobiecka, 2012; Hepel, 2011).

Among sensor methods, SPR is a versatile method for probing the binding of biomolecules through the changes in refractive index occurring on thin metal films. Especially, gold nanoparticles, which are coupled with that of a thin metal surface, are explored to enhance SPR response in biosensors (Gao et al., 2012). In addition, silver nanoparticles produce a much stronger and sharper plasmon resonance in comparison with gold nanoparticles (Pastoriza-Santos and Liz-Marzán, 2008; Wiley et al., 2005). Nonetheless, the structural properties such as poor chemical belonging to silver nanoparticles prevent their broad usage in SPR sensing. Because the plasmonic properties of silver nanoparticles are subject to changes when exposed to water (Jiang et al., 2007; Ying et al., 2007). The other obstacle about silver-based SPR was high susceptibility to oxidation and consequent deterioration of the silver layer coating (Cheng et al., 2015; Moore and Codella, 1988). Therefore, the most common solution was the addition of protective

* Corresponding author.
E-mail address: mlutfi.yola@iste.edu.tr (M.L. Yola).

https://doi.org/10.1016/j.bios.2019.01.053
Received 12 November 2018; Received in revised form 20 January 2019; Accepted 22 January 2019
Available online 31 January 2019
0956-5663/

layer(s) over the silver (Li et al., 2012; Zhai et al., 2007). The important layers were oxides and gold. Especially, a thin protective gold layer was evaporated, forming a bilayered structure. These structures provide stability over bare silver (Xia et al., 2011).

Hexagonal boron nitride nanosheets are known as 2D materials and can be used for sensor applications, catalysis, bioimaging and drug delivery. The large band-gap property of 2D-hBN nanosheets makes them transparent in visible and IR regions. In addition, due to surface area and conductivity, they have significant electrochemical sensor applications (Khan et al., 2016; Weng et al., 2014; Yola and Atar, 2018).

The aim of the study is built up of a novel nanosensor, which is able to determine ETO selectively from urine sample via core-shell nanoparticles (Ag@AuNPs) incorporated hexagonal boron nitride (HBN) nanosheets and MIP. For this purpose, ETO imprinted SPR sensors were prepared and characterized. Ag@AuNPs-HBN nanocomposite was firstly prepared for ETO detection in urine samples. The incorporation between core-shell nanoparticles and HBN nanosheets forms on Lewis acid-base interaction. Lewis base is amine functionalized Ag@AuNPs and Lewis acid is electron-deficient boron atoms on HBN nanosheets.

2. Experimental

2.1. Materials

The materials used in this study were as follows: ETO (Merck, Germany), glucose (GLU) (Merck, Germany), sucrose (SUC) (Merck, Germany), ascorbic acid (ASC) (Merck, Germany), uric acid (UA) (Merck, Germany), citric acid (CA) (Merck, Germany), HEMA (Merck, Germany), MAGA (Merck, Germany), ethylene glycol dimethacrylate (EGDMA) (Merck, Germany), N,N′-azobisisobutyronitrile (AIBN) (Merck, Germany), 2-aminoethanethiol (AET) (Merck, Germany), sodium chloride (NaCl) (Merck, Germany), boron nitride powders (Merck, Germany), potassium ferricyanide ($K_3Fe(CN)_6$) (Merck, Germany). The solutions of ETO, GLU, SUC, ASC, UA and CA (1.0 mM) were prepared in a phosphate buffer solution (PBS) (0.1 M, pH 6.0).

2.2. Instrumentation

The electrochemical experiments were performed by IviumStat (U.S). X-ray diffraction measurements were performed by Rikagu Miniflex X-ray diffractometer. ZEISS EVO 50 (Germany) was utilized for SEM. The ETO detection was carried out by SPR system (GenOptics, SPRi-Lab, Orsay, France) (Yola et al., 2014).

2.3. Preparation of HBN nanosheets and Ag@AuNPs-HBN nanocomposite

HBN nanosheets were firstly developed (Yola and Atar, 2018) and Ag@AuNPs were prepared according to these protocols (Atar et al., 2015; Gupta et al., 2013). To form AET functionalized Ag@AuNPs via the affinity of gold-sulphur, Ag@AuNPs dispersion (1.0 mg/mL) was mixed with AET (0.1 mg/mL) (1:1, v/v) and the mixture was mixed for 10 min and dried at 25 °C (Yola and Atar, 2014). Ultrasonication was utilized for the formation of Ag@AuNPs-HBN nanocomposite. Mixture of HBN nanosheets of 10.0 mg/mL and AET functionalized Ag@AuNPs of 2.0 mg/mL was subjected to ultrasonication for 10 h (Atar and Yola, 2018).

2.4. Modification of SPR chip with AET functionalized Ag@AuNPs-HBN nanocomposite and Development of ETO imprinted sensor on Ag@AuNPs-HBN nanocomposite modified SPR chip

The SPR surface was firstly cleaned with acidic piranha solution (3:1H_2SO_4:H_2O_2, v/v). The surface was dried under vacuum for 2 h. After the clean SPR surface was dipped in AET functionalized Ag@AuNPs-HBN nanocomposite solution (1.0 M), the modified surface was dried under nitrogen atmosphere.

Development of ETO imprinted sensor on Ag@AuNPs-HBN nanocomposite modified SPR chip was carried out: ETO and MAGA monomer (molar ratio is 2:1) were mixed with 250 μL of PBS (pH 6.0) for 2 h. AIBN (5.0 mg) as initiator was dissolved in HEMA (1250 μL) and EGDMA (500 μL). After ETO-MAGA complex (250 μL) was added into the initiator solution, the nitrogen gas was passed into the final solution. 25 μL of final solution was dropped onto the SPR chip with AET functionalized Ag@AuNPs-HBN nanocomposite by using "*spin coating method*" which makes uniform thin films for 15 s. After the polymerization was performed by UV light (365 nm) for 30 min, the chip was dried in vacuum oven. The imprinting selectivity was analyzed by using NIP/Ag@AuNPs-HBN/SPR without ETO.

2.5. ETO removal from chip surface

Owing to the electrostatic forces between MAGA and ETO, 1.0 M NaCl as desorption agent was used in batch system. ETO imprinted polymer on Ag@AuNPs-HBN nanocomposite modified SPR chip (MIP/Ag@AuNPs-HBN/SPR) was dipped into 1.0 M NaCl solution (50 mL). After SPR chip was swinged in bath (250 rpm) at room temperature, the chip was dried with nitrogen gas under vacuum (200 mmHg, 25 °C).

2.6. Procedure of the analysis

The real time determination of ETO was performed using SPR system (GenOptics, SPRi-Lab, Orsay, France). The ETO imprinted sensor on Ag@AuNPs-HBN nanocomposite modified SPR chip was washed with deionized water (50 mL, 2.0 mL min^{-1} flow-rate) and equilibration buffer (pH: 6.0, 0.1 M PBS, 50 mL, 2.0 mL min^{-1} flow-rate). After the ETO-imprinted SPR surface was washed with ultra-pure quality water (5.0 mL) (2.0 mL min^{-1} of flow-rate) and pH 6.0 of 0.1 M PBS (5.0 mL) (2.0 mL min^{-1} of flow-rate), ETO solutions with different concentrations in 0.1 M PBS (pH 6.0) (5 mL) were applied to SPR system (2.0 mL min^{-1} of flow-rate). The changes in resonance frequency were monitored instantly and reached to plateau at about 60 min. The desorption studies were carried out using 1.0 M NaCl solution (5.0 mL) with 2.0 mL min^{-1} of flow-rate. The steps of adsorption–desorption–regeneration were repeated for each ETO concentration.

3. Results and discussion

3.1. The nanostructures' characterization

XRD pattern of bulk boron nitride (curve a) and HBN nanosheets (curve b) were shown in Fig. 1A. The curve a shows the obvious peaks of bulk boron nitride attributing to (100), (101), (102) planes (Hassan et al., 2012). These peaks disappeared on XRD pattern of HBN nanosheets. Nonetheless, (002) plane of boron nitride remains intact (Li et al., 2011). SEM image (Fig. 1B) of boron nitride verified the bulk structure. In this structure, irregular morphology is obtained. After its ultrasonication, the SEM image of the obtained HBN nanosheets (Fig. 1C) shows that the particle thickness of HBN nanosheets decreases in comparison with bulk boron nitride. The presence of Ag@AuNPs on nanopore structure is confirmed on Fig. 1D. The average diameters with 20–25 nm are obtained for core-shell nanoparticles. The B, C, N, S, Au and Ag elements on Ag@AuNPs-HBN nanocomposite confirm the formation of Ag@AuNPs-HBN in the EDX analysis (Fig. 1E). In addition, the morphology of MIP and non-imprinted (NIP) surfaces were investigated. The polymer layer was shown on Fig. 1F for MIP. The less porous structure was seen for NIP in comparison with MIP (Fig. 1G).

3.2. CV and EIS characterization

The reversible peaks with 200 mV of peak potential difference (ΔEp)

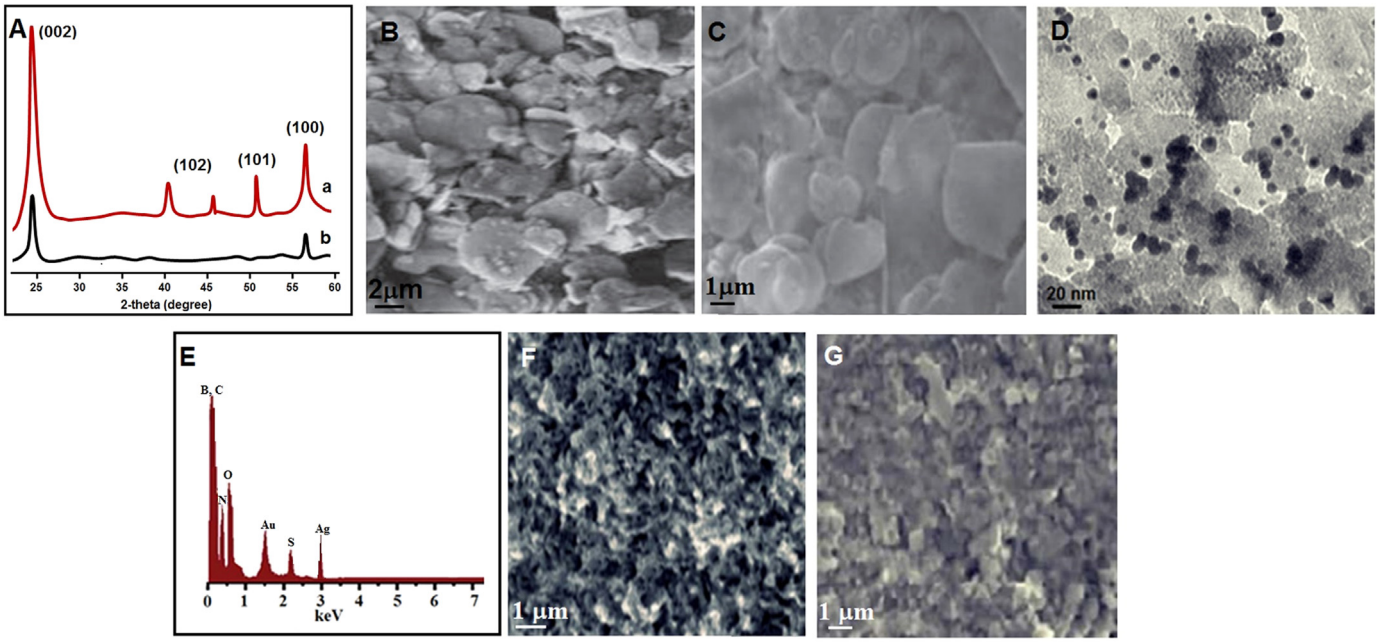

Fig. 1. XRD pattern (A) of bulk boron nitride (curve a) and HBN nanosheets (curve b); SEM images of (B) bulk boron nitride; (C) HBN nanosheets; (D) TEM and (E) EDX images of Ag@AuNPs-HBN nanocomposite; SEM images of (F) MIP/Ag@AuNPs-HBN, (G) NIP/Ag@AuNPs-HBN.

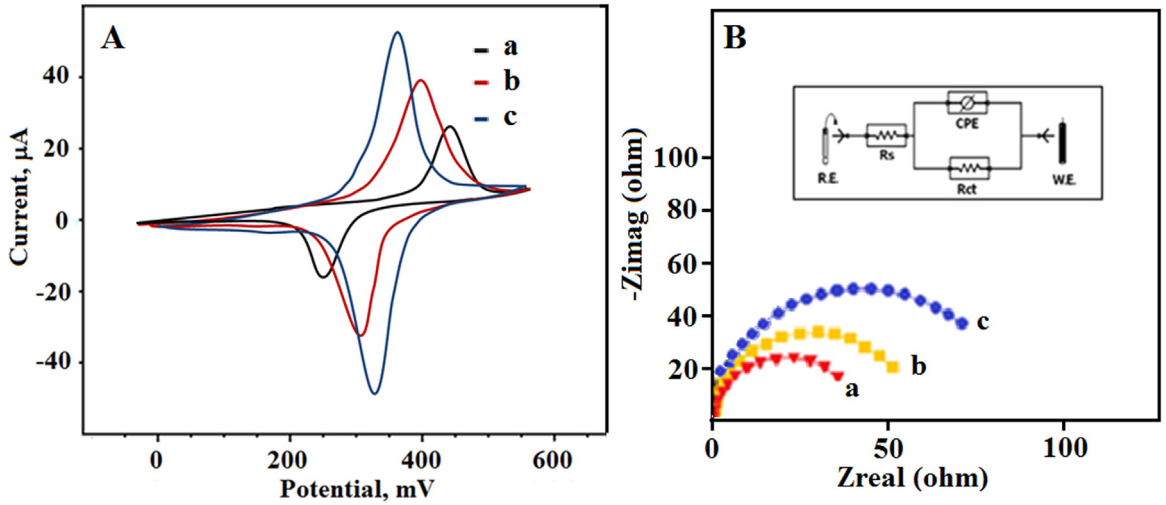

Fig. 2. (A) Cyclic voltammograms at (a) bare GCE, (b) HBN/GCE, (c) Ag@AuNPs-HBN/GCE; (B) EIS response at (a) Ag@AuNPs-HBN/GCE, (b) HBN/GCE, (c) bare GCE; In the presence of 1.0 mM $[Fe(CN)_6]^{3-}$ containing 0.1 M KCl, Scan rate: 200 mV s^{-1}: Frequency range is 100,000 – 0.1 Hz with 10 mV wave amplitude at a formal potential of 0.170 V. RE stands for reference electrode and WE for working electrode.

were obtained for redox probe at bare GCE (curve a of Fig. 2A). ΔEp decreased to 100 mV with obvious increase at HBN/GCE (curve b). Due to the more surface area of HBN nanosheets, the obvious increase was obtained. Its high surface area causes more active sites for 1.0 mM $[Fe(CN)_6]^{3-}$. We can say that the HBN nanosheets can improve catalytic performance towards analyte molecule. The higher current was seen at Ag@AuNPs-HBN/GCE (ΔEp = 50 mV) (curve c). This situation can be explained due to the synergistic effect between boron nitride nanosheets and core-shell nanoparticles (Atar and Yola, 2018). We also calculated the electrode surface areas of these modified surfaces for proving this synergistic effect by using CV method. These areas of bare GCE, HBN/GCE and Ag@AuNPs-HBN/GCE were calculated as 0.170 cm^2, 0.531 cm^2 and 1.339 cm^2, respectively. According to EIS experiments (Fig. 2B), charge transfer resistance (Rct) values are 200 Ω (curve c), 150 Ω (curve b) and 95 Ω (curve a), respectively. Thus, Rct values are in harmony with the results of CV. In addition, Fig. 2B shows the experimental data obtained that are fitted to standard Randles equivalent circuits for Ag@AuNPs-HBN/GCE analysis, which comprizes the solution resistance (R_s), the charge transfer resistance (R_{ct}) and the constant phase element (CPE) for the cases of bare GCE and Ag@AuNPs-HBN/GCE. The experimental impedance values are matched with Randles equivalent circuit simulation using Gamry software (EIS 300 Electrochemical Impedance Spectroscopy Software).

3.3. FTIR and AFM characterization

After ETO removal from Ag@AuNPs-HBN nanocomposite based SPR surface, O–H stretching bands of HEMA and MAGA at 3430 cm^{-1}, saturated C–H stretching bands of MAGA at 2980 cm^{-1}, carboxyl-carbonyl stretching bands of MAGA at 1685 cm^{-1} were obtained in Fig. 3A. In addition, the bands of absorption at 1480 cm^{-1} and 1450 cm^{-1} are related to –COO stretching peaks of MAGA monomer.

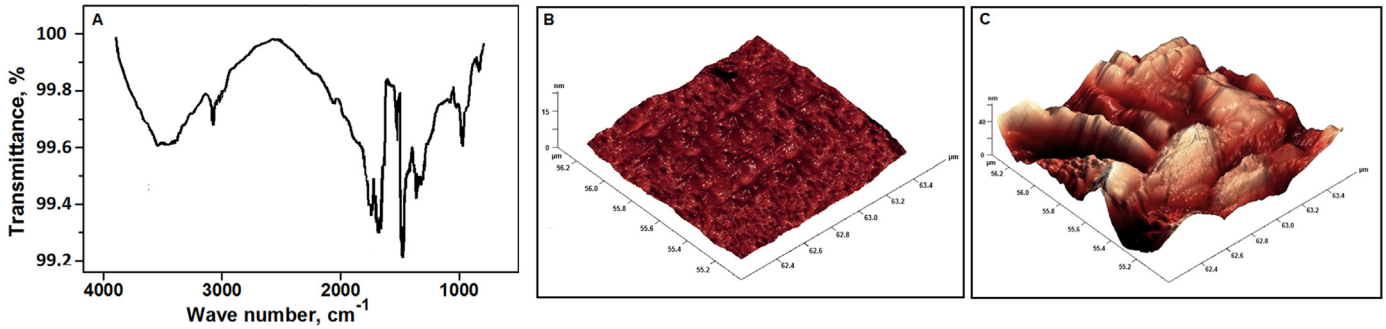

Fig. 3. (A) FTIR spectra of the ETO-imprinted p(HEMA-MAGA) film on Ag@AuNPs-HBN nanocomposite modified SPR surface; AFM images of (B) bare SPR surface; (C) ETO-imprinted p(HEMA-MAGA) film on Ag@AuNPs-HBN nanocomposite modified SPR surface.

The values of surface deepness for bare SPR (Fig. 3B) and ETO-imprinted p(HEMA-MAGA) film on Ag@AuNPs-HBN nanocomposite modified SPR surface (Fig. 3C) are 4.15 ± 0.85 and 34.12 ± 0.53 nm, respectively. The results show that the polymerization on nanocomposite modified SPR surface is accomplished.

3.4. Effect of different MIP sensors on SPR signals

Fig. S1A shows the effects of different MIP sensors such as MIP/SPR, MIP/HBN/SPR, MIP/AuNPs-HBN/SPR and MIP/Ag@AuNPs-HBN/SPR on signals. According to Fig. S1A, the highest SPR signals were obtained by using MIP/Ag@AuNPs-HBN/SPR in the presence of 1.0 ng mL^{-1} ETO. This situation is in harmony with the results of CV and EIS. Because of the synergistic effect between boron nitride nanosheets and core-shell nanoparticles (Atar and Yola, 2018), the optimum sensor signal was obtained on MIP/Ag@AuNPs-HBN/SPR.

3.5. Effect of pH on SPR signals

Buffer solutions with different pH were tested (Fig S1B). The responses towards SPR sensors increase gradually up to pH 6.0. Due to MAGA monomer which is based on glutamic acid (pKa_1: 2.10, pKa_2: 4.07), the carboxylic acid groups of monomer loaded negatively with the increase in pH value. These groups effectively interacted with polar groups of ETO. Owing to this situation, the affinity of sensor-analyte increased. However, after pH 6.0, the conversion of ETO to its anion form occurred and the affinity of sensor-analyte decreased. Thus, the optimum pH value in this study is pH 6.0 (ΔR = 11.413) in presence of 1.0 ng mL^{-1} ETO (Fig S1C).

3.6. Linearity range

Fig. 4 shows the relationship between SPR signals and ETO amount at MIP/Ag@AuNPs-HBN/SPR (from blank solution to 1.00 ng mL^{-1} ETO). The regression equation is as y (ΔR) = 11.073 × (ng mL^{-1})

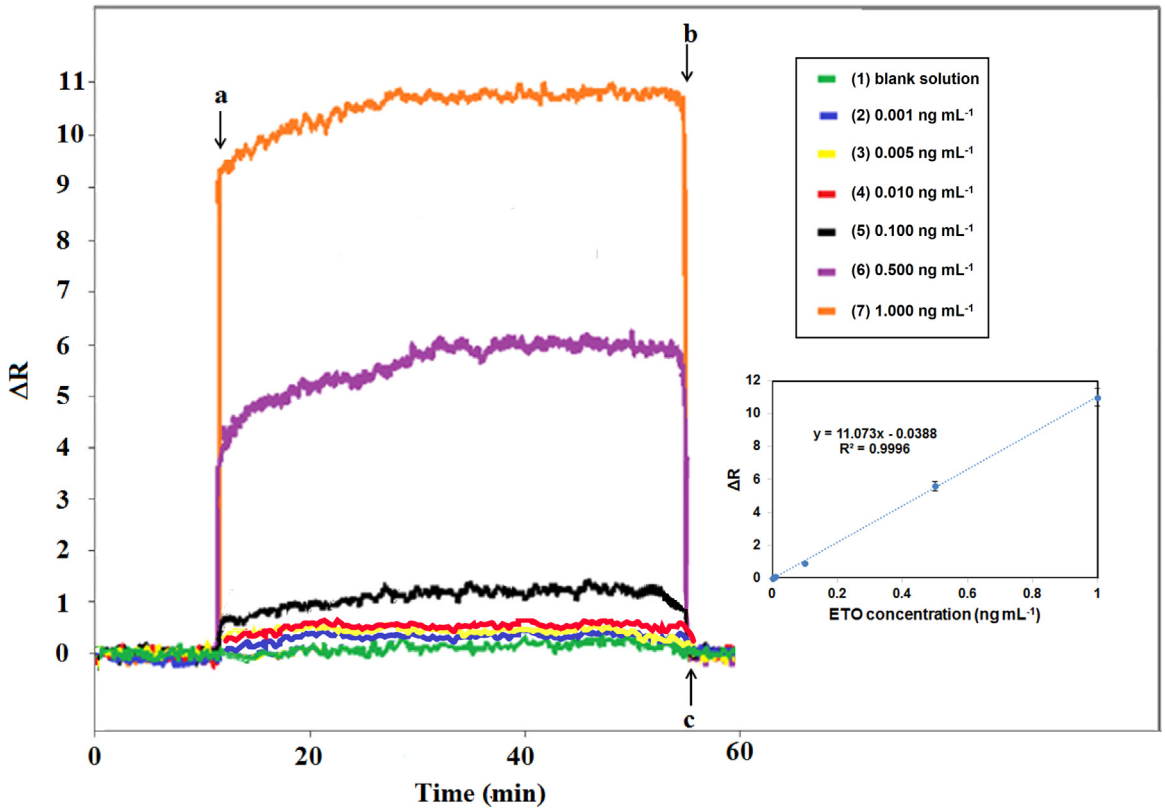

Fig. 4. Effect of ETO concentration on the SPR signals: Inset: Calibration curve of ETO concentrations at MIP/Ag@AuNPs-HBN/SPR in the presence of pH 6.0 of PBS (from blank solution to 1.00 ng mL^{-1} ETO): (a) adsorption; (b) desorption; (c) regeneration.

Table 1
Comparison of MIP/Ag@AuNPs-HBN/SPR with the other methods.

Material	Linear Range (mol L^{-1})	LOD (mol L^{-1})	Ref.
Au/Pd@rGO	1.00×10^{-8}–4.00×10^{-5}	7.18×10^{-10}	(Hatamluyi et al., 2018)
MWCNT/GCE	2.00×10^{-8}–2.00×10^{-6}	5.00×10^{-9}	(Bozal-Palabiyik et al., 2013)
CQDs/GCE	2.00×10^{-8}–1.00×10^{-5}	5.00×10^{-9}	(Nguyen et al., 2016)
CPE	2.50×10^{-7}–1.00×10^{-5}	1.00×10^{-7}	(Radi et al., 2007)
GNWs	5.00×10^{-8}–5.00×10^{-5}	4.36×10^{-9}	(Tzouvadaki et al., 2018)
RP-HPLC	1.70×10^{-6}–1.70×10^{-4}	5.10×10^{-7}	(Agwa et al., 2018)
MIP/Ag@AuNPs-HBN/SPR	***1.70×10^{-12} –1.70×10^{-9}***	***4.25×10^{-13}***	***This study***

Au/Pd@rGO: gold/palladium@reduced graphene oxide; MWCNT/GCE: Multi-walled carbon nanotube modified glass carbon electrode; CQDs/GCE: Carbon quantum dot modified glassy carbon electrode; CPE: Carbon paste electrode; GNWs: Graphene nanowalls; RP-HPLC: rapid reversed-phase high-performance liquid chromatography; MIP/Ag@AuNPs-HBN/SPR: SPR sensor based on core-shell nanoparticles incorporated hexagonal boron nitride nanosheets.

− 0.0388 for MIP. Hence, this study has shown that MIP/Ag@AuNPs-HBN/SPR was found to be more sensitivity to ETO analyte (Inset of Fig. 4). 0.001 ng mL^{-1} and 0.00025 ng mL^{-1} were found as quantification limit (LOQ) and LOD Moreover, Table 1 presented the comparisons between the MIP/Ag@AuNPs-HBN/SPR and other systems. Finally, MIP/Ag@AuNPs-HBN/SPR was found to reveal higher sensitivity in comparison with other analytical methods.

3.7. Recovery

The recovery percentage values ranged between 99.30% and 100.72% with relative standard deviation < 1.00 (Table 1S). Recovery values were calculated by the equation:

$$\text{Recovery} = \frac{\text{Found amount(ng mL}^{-1})}{\text{Actual amount(ng mL}^{-1})} \times 100$$

Closeness of the results to 100.00% showed that the developed nanosensor was found to have a high selectivity. In addition, Fig. S2 showed SPR sensorgrams of the spiked samples for recovery test. The calibration equation of standard addition method is as y (ΔR) = 11.013 × (ng mL^{-1}) + 0.149 for MIP/Ag@AuNPs-HBN/SPR. On the other hand, no significance difference between the slopes of regression equations of linear calibration technique and standard addition method was found. Subsequently, the selective analysis of ETO is completed successfully on MIP/Ag@AuNPs-HBN/SPR.

3.8. Selectivity, stability, repeatability, reproducibility and reusability of MIP/Ag@AuNPs-HBN/SPR

To confirm the selectivity of the ETO-imprinted SPR nanosensor against 1.0 ng mL^{-1}ETO in urine samples in the presence of 1.0 ng mL^{-1} GLU, 1.0 ng mL^{-1} SUC, 1.0 ng mL^{-1} ASC, 1.0 ng mL^{-1} UA and 1.0 ng mL^{-1} CA as competitors (Fig. 5A), the samples were applied to the nanosensors. The selectivity coefficients (k) and relative selectivity coefficients (k′) values are given in Table 2S. MIP/Ag@AuNPs-HBN/SPR was 4.0, 6.0, 12.0, 24.0 and 48.0 times selective towards ETO in comparison with GLU, SUC, ASC, UA and CA. The results show that because of selective cavities in the polymer structure, ETO-imprinted SPR nanosensor has higher adsorption capacity (ΔR values) for ETO in comparison to GLU, SUC, ASC, UA and CA.

To display the specificity of ETO-imprinted SPR nanosensor, non-imprinted SPR nanosensor (NIP) was also prepared and the signals of non-imprinted SPR nanosensor against 1.0 ng mL^{-1}ETO, 1.0 ng mL^{-1} GLU, 1.0 ng mL^{-1} SUC, 1.0 ng mL^{-1} ASC, 1.0 ng mL^{-1} UA and 1.0 ng mL^{-1} CA were obtained as 1.00, 0.80, 0.60, 0.40. 0.20 and 0.10, respectively (Fig. 5B). The selectivity coefficients for non-imprinted SPR nanosensor in respect to 1.0 ng mL^{-1} GLU, 1.0 ng mL^{-1} SUC, 1.0 ng mL^{-1} ASC, 1.0 ng mL^{-1} UA and 1.0 ng mL^{-1} CA were calculated as 1.25, 1.67, 2.50, 5.00 and 10.00, respectively. The results for relative selectivity constants showing selectivity gained by imprinting process display that ETO-imprinted SPR nanosensor was 3.20, 3.59, 4.80, 4.80 and 4.80 times more selective in comparison to GLU, SUC, ASC, UA and CA, respectively.

The signals of 1.0 ng mL^{-1} ETO were measured for the stability of MIP/Ag@AuNPs-HBN/SPR during 60 days and the repeatable responses at about (ΔR = 11.00 with 0.17% of relative standard deviation) were observed. Thus, the imprinted sensor has good stability. The five cycles (equilibration-adsorption-regeneration) were performed in presence of 1.0 ng mL^{-1} ETO for repeatability test and the repeatable responses at about (ΔR = 11.00 with 0.21% of relative standard deviation) were observed during the cycles (Fig. 5C).

The reproducibility test was performed with ten different ETO-imprinted SPR nanosensor. These imprinted nanosensors were fabricated independently by using the same procedure. The relative standard deviation value was found to be 0.34% for SPR signal in the presence of 1.0 ng mL^{-1} ETO and it indicated the reliability of nanosensor

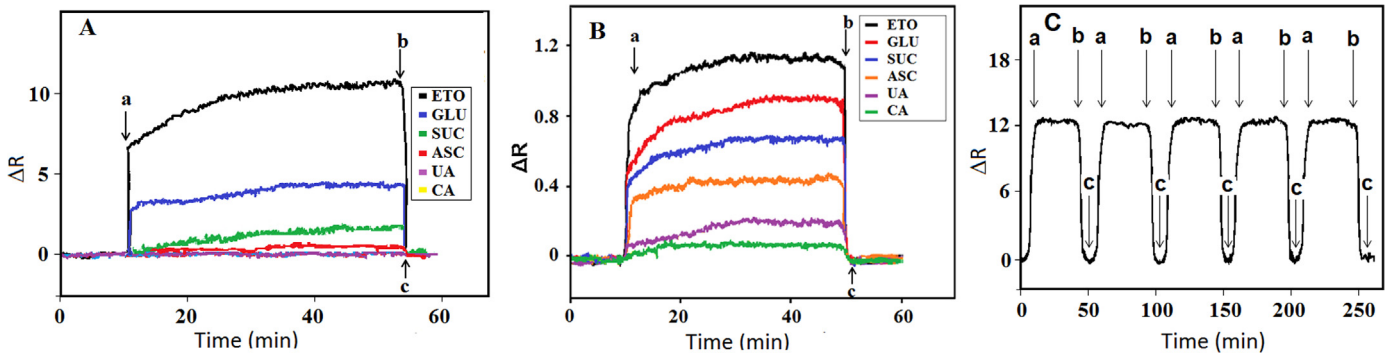

Fig. 5. Comparison of selectivity of SPR sensors: (A) Sensorgrams relating to 1.0 ng mL^{-1} ETO, GLU, SUC, ASC, UA and CA on MIP/Ag@AuNPs-HBN/SPR in the presence of pH 6.0 of PBS (a) adsorption; (b) desorption; (c) regeneration; (B) Sensorgrams relating to 1.0 ng mL^{-1} ETO, GLU, SUC, ASC, UA and CA on NIP/Ag@AuNPs-HBN/SPR in the presence of pH 6.0 of PBS (a) adsorption; (b) desorption; (c) regeneration; (C) Repeatability of MIP/Ag@AuNPs-HBN/SPR: Analyte concentration: 1.0 ng mL^{-1} ETO in the presence of pH 6.0 of PBS: (a) adsorption; (b) desorption; (c) regeneration.

preparation procedure.

Finally, the reusability of ETO-imprinted SPR nanosensor was examined. According to the results, ETO-imprinted SPR nanosensor was not found as a disposable sensor. It could be used at least 30 times (relative standard deviation was 0.44%) after washing with 0.1 M PBS (pH 6.0).

4. Conclusion

In this study, we have combined the advantages of core-shell nanoparticles incorporated HBN nanosheets and molecular imprinting for detection of anticancer drug. The nanomaterials were characterized by SEM, TEM, XRD, EDX, CV and EIS. 1.70×10^{-12}–1.70×10^{-9} M and 4.25×10^{-13} M were found as the linearity range and LOD for the developed SPR nanosensor. The developed nanosensor also shows high selectivity, stability and repeatability in urine sample. According to the recovery experiments and standard addition technique, it could be stated that the matrix presence in urine sample had no effect on the selective analysis of anticancer drug. In addition, the developed SPR nanosensor was found to be stable, repeatable and reusable. Finally, the prepared SPR nanosensor showed high selectivity and sensitivity in urine samples in comparison with other analytical methods.

Credit author statement

Mehmet Lütfi YOLA conceived the original idea and wrote the manuscript. Abdullah ÖZKAN fabricated the Etoposide imprinted SPR nanosensor with help from Necip ATAR. Mehmet Lütfi YOLA supervised the project.

Declaration-of-competing-interests

The paper is original and is not published previously in whole or a part and not being considered elsewhere

Appendix A. Supporting information

Supplementary data associated with this article can be found in the online version at doi:10.1016/j.bios.2019.01.053.

References

Agwa, M.M., Elessawy, F.M., Hussein, A., El Demellawy, M.A., Elzoghby, A.O., Abd El-Salam, M.H., Eldiwany, A.I., 2018. Anal. Methods 10 (19), 2272–2280.

Atar, N., Eren, T., Demirdögen, B., Yola, M.L., Çağlayan, M.O., 2015. Ionics 21 (8), 2285–2293.

Atar, N., Yola, M.L., 2018. J. Electrochem. Soc. 165 (5), H255–H262.

Bozal-Palabiyik, B., Dogan-Topal, B., Uslu, B., Can, A., Ozkan, S.A., 2013. J. Solid State Electrochem. 17 (11), 2815–2822.

Cheng, Z., Wang, Z., Gillespie, D.E., Lausted, C., Zheng, Z., Yang, M., Zhu, J., 2015. Anal. Chem. 87 (3), 1466–1469.

Gao, C., Lu, Z., Liu, Y., Zhang, Q., Chi, M., Cheng, Q., Yin, Y., 2012. Angew. Chem. Int. Ed. 51 (23), 5629–5633.

Gong, X., Yang, L., Zhang, F., Liang, Y., Gao, S., Liu, K., Chen, W., 2017. Biomed. Chromatogr. 31 (11), e3989.

Gupta, V.K., Atar, N., Yola, M.L., Eryılmaz, M., Torul, H., Tamer, U., Boyacı, İ.H., Üstündağ, Z., 2013. J. Colloid Interface Sci. 406, 231–237.

Hassan, J.J., Mahdi, M.A., Kasim, S.J., Ahmed, N.M., Abu Hassan, H., Hassan, Z., 2012. Appl. Phys. Lett. 101, 261108.

Hatamluyi, B., Lorestani, F., Es'haghi, Z., 2018. Biosens. Bioelectron. 120, 22–29.

Hepel, M., Stobiecka, M., 2012. Detection of oxidative stress biomarkers using functional gold nanoparticles. In: Matijevic, E. (Ed.), Fine Particles in Medicine and Pharmacy. Springer Sci. Publ., New York, pp. 241–281.

Hepel, S., 2011. Detection of oxidative stress biomarkers using novel nanostructured biosensors. In: Serra, P.A. (Ed.), New Perspectives in Biosensors Technology and Applications. INTECH, Vienna, pp. 343–372.

Jiang, X., Zeng, Q., Yu, A., 2007. Langmuir 23 (4), 2218–2223.

Kamal, A., Singh, M., Ahmad, F.J., Saleem, K., Ahmad, S., 2017. Arab. J. Chem. 10, S2539–S2546.

Khan, A.F., Brownson, D.A.C., Randviir, E.P., Smith, G.C., Banks, C.E., 2016. Anal. Chem. 88 (19), 9729–9737.

Li, C.-T., Lo, K.-C., Chang, H.-Y., Wu, H.-T., Ho, J.H., Yen, T.-J., 2012. Biosens. Bioelectron. 36 (1), 192–198.

Li, L.H., Chen, Y., Behan, G., Zhang, H., Petravic, M., Glushenkov, A.M., 2011. J. Mater. Chem. 21 (32), 11862–11866.

Medetalibeyoğlu, H., Manap, S., Yokuş, Ö.A., Beytur, M., Kardaş, F., Akyıldırım, O., Özkan, V., Yüksek, H., Yola, M.L., Atar, N., 2018. J. Electrochem. Soc. 165 (5), F338–F341.

Moore, W.M., Codella, P.J., 1988. J. Phys. Chem. 92 (15), 4421–4426.

Nguyen, H.V., Richtera, L., Moulick, A., Xhaxhiu, K., Kudr, J., Cernei, N., Polanska, H., Heger, Z., Masarik, M., Kopel, P., Stiborova, M., Eckschlager, T., Adam, V., Kizek, R., 2016. Analyst 141 (9), 2665–2675.

Pang, S., Zheng, N., Felix, C.A., Scavuzzo, J., Boston, R., Blair, I.A., 2001. J. Mass Spectrom. 36 (7), 771–781.

Pastoriza-Santos, I., Liz-Marzán, L.M., 2008. J. Mater. Chem. 18 (15), 1724–1737.

Poole, C.J., Earl, H.M., Hiller, L., Dunn, J.A., Bathers, S., Grieve, R.J., Spooner, D.A., Agrawal, R.K., Fernando, I.N., Brunt, A.M., O'Reilly, S.M., Crawford, S.M., Rea, D.W., Simmonds, P., Mansi, J.L., Stanley, A., Harvey, P., McAdam, K., Foster, L., Leonard, R.C.F., Twelves, C.J., 2006. N. Engl. J. Med. 355 (18), 1851–1862.

Radi, A.E., Abd-Elghany, N., Wahdan, T., 2007. Chem. Pharm. Bull. 55 (9), 1379–1382.

Stobiecka, M., Deeb, J., Hepel, M., 2009. ECS Trans. 19 (28), 15–32.

Tzouvadaki, I., Aliakbarinodehi, N., Dávila Pineda, D., De Micheli, G., Carrara, S., 2018. Sens. Actuators B 262, 395–403.

Weng, Q., Wang, B., Wang, X., Hanagata, N., Li, X., Liu, D., Wang, X., Jiang, X., Bando, Y., Golberg, D., 2014. ACS Nano 8 (6), 6123–6130.

Wiley, B., Sun, Y., Mayers, B., Xia, Y., 2005. Chem. Eur. J. 11 (2), 454–463.

Xia, L., Yin, S., Gao, H., Deng, Q., Du, C., 2011. Plasmonics 6 (2), 245–250.

Xu, J., Zhou, Y., Zhang, J., Chen, Y., Zhuang, R., Liu, T., Cai, W., 2012. Clin. Chim. Acta 413 (15), 1284–1287.

Ying, C., Chungang, W., Zhanfang, M., Zhongmin, S., 2007. Nanotechnology 18 (32), 325602.

Yola, M.L., Atar, N., 2014. Electrochim. Acta 119, 24–31.

Yola, M.L., Atar, N., 2018. J. Electrochem. Soc. 165 (14), H897–H902.

Yola, M.L., Eren, T., Atar, N., 2014. Sens. Actuators B 195, 28–35.

Yola, M.L., Eren, T., Atar, N., 2016. J. Electrochem. Soc. 163 (13), B588–B593.

Zhai, P., Guo, J., Xiang, J., Zhou, F., 2007. J. Phys. Chem. C 111 (2), 981–986.